Phase Transitions
Vol. 83, No. 2, February 2010, 140–158

Taylor & Francis
Taylor & Francis Group

Mass-transport models with fragmentation and aggregation

Gaurav P. Shrivastav[a], Varsha Banerjee[b] and Sanjay Puri[a]*

[a]*School of Physical Sciences, Jawaharlal Nehru University, New Delhi – 110067, India;*
[b]*Department of Physics, Indian Institute of Technology, Hauz Khas, New Delhi – 110016, India*

(*Received 19 November 2009; final version received 14 December 2009*)

We present a review of nonequilibrium phase transitions in mass-transport models with kinetic processes like fragmentation, diffusion, aggregation, etc. These models have been used extensively to study a wide range of physical problems. We provide a detailed discussion of the analytical and numerical techniques used to study mass-transport phenomena.

Keywords: mass transport models; *k*-chip fragmentation and aggregation; steady-state; mean field theory; Monte Carlo simulations

1. Introduction

There has been intense research interest in phase transitions in mass-transport and growth models involving adsorption and desorption, fragmentation, diffusion, and aggregation. These processes are ubiquitous in nature and arise in a large number of seemingly diverse systems such as growing interfaces [1,2], colloidal suspensions [3], polymer gels [4], river networks [5], granular materials [6], traffic flows [7], etc. In these systems, different nonequilibrium states arise if the rates of the underlying microscopic processes are varied. Conservation laws also play an important role in determining both the time-dependent behavior and steady states of such systems. As these steady states are usually not described by the Gibbs distribution, they are hard to determine. However, much insight on this issue has been gained by studying lattice models. Due to their simplistic nature, these models can be treated either exactly or via a mean-field (MF) approach [8–13]. They are also simple to implement numerically using Monte Carlo (MC) techniques [14,15].

In this article, we present a pedagogical discussion of the modeling and simulation of mass-transport and growth phenomena. We discuss analytical and numerical techniques in the context of mass-transport models where the elementary move is the fragmentation of mass k, and its subsequent diffusion to a neighboring site where it aggregates. The k-chip models that we study here are interesting in physical situations where the deposited material consists of polymers. We study the MF limit of these models, focusing on the steady-state mass distribution ($P(m)$ *vs.* m), which is characterized by k branches. We also compare the MF results with MC simulations in $d = 1, 2$.

This article is organized as follows. In Section 2, we present a framework for mass-transport models in terms of the rate (evolution) equations for $P(m, t)$, the

*Corresponding author. Email: puri@mail.jnu.ac.in

ISSN 0141–1594 print/ISSN 1029–0338 online

DOI: 10.1080/01411590903553460
http://www.informaworld.com

probability that a site has mass m at time t. We then discuss various systems which can be described within this framework. In Section 3, we introduce k-chip models and obtain analytical results for the MF versions of these models. In Section 4, we present MC results for mass-transport models, and compare them with the corresponding MF solutions. We conclude this article with a summary and discussion in Section 5. The appendices contain details of calculations and MC procedures.

2. Framework and applications of mass-transport models

2.1. *Lattice models and rate equations*

We consider lattice models of mass transport with the processes of fragmentation, diffusion and aggregation. For simplicity, we describe the models on a one-dimensional lattice with periodic boundary conditions (the generalization to higher dimensions is straightforward). To begin with, masses are placed randomly at each site with an overall mass density ρ. Let $m_i(t)$ be the mass at site i at time t. The mass variables assume discrete values 0, 1, 2, 3, etc. The evolution of the system is as follows. A piece of mass n chips off a site having mass m ($\geq n$) with rate $g_m(n)$. This piece deposits on the right neighbor with probability p, or on the left neighbor with probability $1-p$. The mass of the chosen neighbor adds up, while that of the departure site decreases, with the total mass of the system remaining conserved. Figure 1 is a schematic depiction of the above model. To facilitate MC simulations, the update rules can be rewritten as follows:

(1) Randomly pick a site i at time t with mass $m_i(t)=m$. The site is updated as $m_i(t+1)=m_i(t)-n$ with rate $g_m(n)$.
(2) The neighboring sites are updated as $m_{i+1}(t+1)=m_{i+1}(t)+n$ with probability p, or $m_{i-1}(t+1)=m_{i-1}(t)+n$ with probability $1-p$.

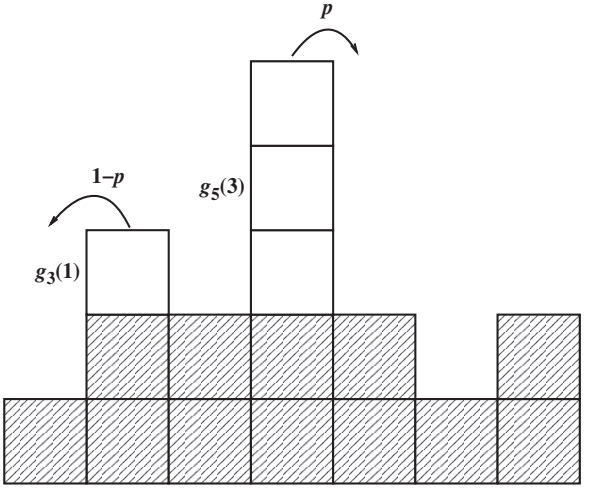

Figure 1. Schematic representation of the conserved-mass model with fragmentation and aggregation. A mass n can chip from a site with mass m with a fragmentation rate $g_m(n)$, and aggregate with the right (left) neighbor with probability p ($1-p$).

We also study the above models within an MF approximation which keeps track of the distribution of masses, ignoring correlations in the occupancy of adjacent sites. Although the MF theory has this shortcoming, our MC simulations show that it gives an accurate description of the above model, even in the one-dimensional case. Let $P(m,t)$ denote the probability that a site has mass m at time t. In the MF limit, $P(m,t)$ evolves as follows:

$$\frac{\mathrm{d}}{\mathrm{d}t}P(m,t) = -P(m,t)\sum_{m_1=1}^{m} g_m(m_1) - P(m,t)\sum_{m_2=1}^{\infty} P(m_2,t)\sum_{m_1=1}^{m_2} g_{m_2}(m_1) + \sum_{m_1=1}^{\infty} P(m+m_1,t)\, g_{m+m_1}(m_1) + \sum_{m_1=1}^{m} P(m-m_1,t)\sum_{m_2=m_1}^{\infty} P(m_2,t)\, g_{m_2}(m_1), \quad m \geq 1, \tag{1}$$

$$\frac{\mathrm{d}}{\mathrm{d}t}P(0,t) = -P(0,t)\sum_{m_2=1}^{\infty} P(m_2,t)\sum_{m_1=1}^{m_2} g_{m_2}(m_1) + \sum_{m_1=1}^{\infty} P(m_1,t)\, g_{m_1}(m_1). \tag{2}$$

These equations enumerate all possible ways in which a site with mass m may change its mass. The first term on the right-hand side (RHS) of Equation (1) is the "loss" of mass m due to chipping, i.e., a site with mass m may lose a fragment of mass m_1 ($\leq m$) to a neighbor. The second term on the RHS represents the loss due to transfer of mass from a neighbor chipping. The third and fourth terms are the 'gain' terms which represent the ways in which a site with mass greater (lesser) than m can lose (gain) the excess weight (deficit) to yield mass m. The terms of Equation (2) can be interpreted similarly. In order to ensure that all loss and gain terms have been included in the rate equations, it is useful to check the sum rule

$$\frac{\mathrm{d}}{\mathrm{d}t}\sum_{m=0}^{\infty} P(m,t) = 0 \quad \text{or} \quad \sum_{m=0}^{\infty} P(m,t) = 1. \tag{3}$$

With some algebra, it can be shown that Equations (1) and (2) do indeed satisfy the above rule. We provide the steps for this check in Appendix A.

If other microscopic processes are present, additional terms will have to be included in the rate equations (1) and (2). For example, if adsorption of a unit mass at a site occurs with rate q, we require additional terms $-qP(m,t)$ and $+qP(m-1,t)$ in Equation (1), and $-qP(0,t)$ in Equation (2). While it is simple to write realistic rate equations by including all relevant microscopic processes, it is often difficult to solve them analytically to obtain either time-dependent or steady-state solutions.

Several MF models studied earlier may be obtained as special cases of Equations (1) and (2) by an appropriate choice of the chipping kernel $g_m(n)$. Some interesting issues which have been addressed in these studies, in addition to obtaining steady-state mass distributions, are the possibilities of phase transitions in these models. We mention two representative examples to highlight the typical questions which are addressed in this area.

(1) Majumdar et al. [11] studied a conserved-mass model in which either a single unit or the entire mass could dissociate from a site. Thus, $g_m(n)$ has the form

$$g_m(n) = w\delta_{n,1} + \delta_{n,m}, \tag{4}$$

where w is the relative rate of the 1-chip process. The corresponding rate equations are obtained by substituting Equation (4) in Equations (1) and (2) as follows:

$$\frac{\mathrm{d}}{\mathrm{d}t}P(m,t) = -(1+w)(1+s_1)P(m,t) + wP(m+1,t) + ws_1P(m-1,t) + \sum_{m_1=1}^{m} P(m-m_1,t)P(m_1,t), m \geq 1, \tag{5}$$

$$\frac{d}{\mathrm{d}t}P(0,t) = -(1+w)s_1P(0,t) + wP(1,t) + s_1, \tag{6}$$

where $s_1 = \sum_{m=1}^{\infty} P(m,t)$.

The steady-state mass distributions ($P(m)$ *vs.* m) for Equations (5) and (6) were calculated by Majumdar et al. as a function of the density $\rho = \langle m \rangle$ of the system. The relevant analytical techniques are described in Section 3. They observed a *dynamical phase transition* as ρ was varied (w being fixed), with the different phases being characterized by different steady-state distributions. For $\rho < \rho_c(w)$, $P(m)$ decayed exponentially for large m. For $\rho = \rho_c(w)$, $P(m)$ showed a power-law decay, $P(m) \sim m^{-\tau}$ with a universal exponent $\tau = 5/2$. Finally, the "high-density" phase arising for $\rho > \rho_c(w)$ was characterized by the formation of an infinite aggregate (at $m = \infty$). The aggregate coexisted with smaller clusters, and their mass distribution showed a power-law decay, $P(m) \sim m^{-\tau}$.

(2) Rajesh et al. [12] studied a system of fragmenting and coagulating particles with mass-dependent diffusion rates. In this model,

$$g_m(n) = w\delta_{n,1} + m^{-\alpha}\delta_{n,m}. \tag{7}$$

The case $\alpha = 0$ corresponds to the model in Equation (4). The corresponding rate equations are

$$\frac{\mathrm{d}}{\mathrm{d}t}P(m,t) = -(w + m^{-\alpha} + ws_1 + \overline{s}_1)P(m,t) + wP(m+1,t) + ws_1P(m-1,t) + \sum_{m_1=1}^{m} \frac{P(m-m_1,t)P(m_1,t)}{m_1^{\alpha}}, m \geq 1, \tag{8}$$

$$\frac{\mathrm{d}}{\mathrm{d}t}P(0,t) = -(ws_1 + \overline{s}_1)P(0,t) + wP(1,t) + \overline{s}_1, \tag{9}$$

where $\overline{s}_1 = \sum_{m=1}^{\infty} m^{-\alpha}P(m,t)$.

For $\alpha > 0$, Rajesh et al. showed that there is no dynamical phase transition. The high-density phase with an infinite aggregate disappears, although its imprint in the form of a large aggregate is observed in finite systems. Further, the steady-state probability distribution $P(m)$ decays exponentially with m for all ρ and $\alpha > 0$.

Before concluding this discussion, a few words regarding the condensation transition are in order. The condensation observed in the model in Equations (5) and (6) occurs due to the dynamical rules of evolution and not due to an "attraction" between the masses. Though it shares analogies with *Bose–Einstein condensation* (BEC), an important difference is that these condensates are formed in real space rather than momentum space, as is the case of BEC. As a matter of fact, condensation occurs in a variety of seemingly diverse systems which are governed by nonequilibrium dynamics [11].

2.2. *Some applications of mass-transport models*

We now discuss some physical applications of mass-transport models. The aim here is to stress the general nature of the questions addressed in a variety of physical situations involving mass transport.

2.2.1. *Magnetic nanoparticles*

Recently, there has been much research interest in suspensions of single-domain *magnetic nanoparticles* (MNP), which have a wide range of technological applications, e.g., memory devices, magnetic resonance imaging, targeted drug delivery, bio-markers, and bio-sensors [16,17]. A major reason for the utility of MNPs is the ease with which they can be detected and manipulated by an external magnetic field. Their response times are strongly size-dependent, thus introducing the possibility of controlling particle sizes to obtain desired response times.

An inherent property of MNP suspensions is cluster formation, due to the presence of attractive interactions of varying strengths between the constituent particles [18]. Therefore, mass-transport models with fragmentation and aggregation have been traditionally employed to study clustering dynamics in these systems. The steady-state cluster-size distributions and the average cluster size are determined by the interplay between aggregation (due to attractive interactions) and fragmentation (due to repulsive interactions and thermal noise) [18]. Assuming that the number of particles is N, and denoting the number of clusters containing k particles at time t by $c(k,t)$, the rate equations in the MF approximation are as follows [19]:

$$\frac{\partial}{\partial t}c(k,t) = \frac{1}{2}\sum_{i,j=1}^{\infty}\delta_{k,i+j}K_{ij}c(i,t)c(j,t) - c(k,t)\sum_{j=1}^{\infty}K_{kj}c(j,t) + f_{k+1}c(k+1,t) - f_k c(k,t) + \delta_{k,1}\sum_{j=1}^{\infty}f_j c(j,t), \quad k \geq 1. \tag{10}$$

In Equation (10), K_{ij} and f_k are the aggregation and fragmentation kernels, respectively. The aggregation kernel describes the coalescence of two clusters containing i and j particles to yield a larger cluster with $k = i + j$ particles. In many models, it is assumed to have a mass-dependent form, $K_{ij} = D(i^{-\mu} + j^{-\mu})$. This accounts for the reduced mobility of large clusters. The fragmentation kernel f_k describes the loss of one particle from a cluster with k particles, and has also been assumed to have a mass-dependent form, $f_k = wk^{\nu}$. Equation (10) can be rewritten in terms of probability distributions (cf. Equations (1) and (2)) by introducing a normalization factor, $P(k,t) = c(k,t)/\sum_{k=1}^{\infty}c(k,t)$.

2.2.2. *Traffic models*

Our second example is in the context of traffic models. In this context, we discuss the so-called *Bus Route Model* (BRM) [20]. Here, one is interested in the initial conditions or parameters which result in a clustering of buses or a traffic jam. The model is defined on a one-dimensional lattice of size L. Each site i has two associated variables τ_i and ϕ_i: (i) If a site i is occupied by a bus, $\tau_i = 1$; otherwise $\tau_i = 0$. (ii) If a site i has passengers, then $\phi_i = 1$; otherwise $\phi_i = 0$. A site cannot have both $\tau_i = \phi_i = 1$, i.e., $\tau_i + \phi_i \leq 1$. If there are M buses, the bus density $\rho = M/L$ is a conserved quantity. However, the total number of sites with passengers is not conserved.

The update rules are as follows: (i) Pick a site i at random. (ii) If $\tau_i = \phi_i = 0$, then set $\phi_i = 1$ with rate λ, i.e., a passenger arrives at an empty site with rate λ. (iii) If $\tau_i = 1$ and $\tau_{i+1} = 0$, a bus hops onto a site with no passengers ($\phi_{i+1} = 0$) with rate α, and to a site with passengers ($\phi_{i+1} = 1$) with rate β. Thus, the variables $\tau_i \to 0$ and $\tau_{i+1} \to 1$ and $\phi_{i+1} \to 0$ with rate α or β, as the case may be. Usually, $\beta < \alpha$ as the buses slow down when passengers are being picked up. A jam in the system is a gap between buses of size $x \sim O(L)$, which is stable in the thermodynamic limit.

The MF approximation of this model considers the distribution of gaps $P(x, t)$, ignoring the time-correlations in the hopping of buses. It should be noted here that, unlike the mass-transport models described in Section 2.1, the BRM is asymmetric. Thus, the movement of the buses is unidirectional although the hop rate is proportional to the size of the gap. These features put the BRM in a class of models which are referred to as *zero-range processes* (ZRP) [21]. The important property of a ZRP is that it yields a steady-state as a product of marginals calculated using well-defined procedures [22]. Further, MF calculations are exact for this class of models.

From simulations of the discrete model, heuristic arguments and MF theory, O'Loan et al. obtain evidence of a jamming transition as a function of the density of buses ρ. In terms of buses and passengers, the jam may be interpreted as follows. An ideal situation is one where the buses are evenly distributed along the route so that each bus picks up approximately the same number of passengers. Jamming or clustering of buses may occur if one of the buses gets delayed due to some fluctuation at a pick-up point. Subsequently, the buses which follow catch up with the delayed bus result in a jam! An important observation here is that the jamming is a consequence of a local, stochastic dynamics, which couples the conserved variable (buses) and the nonconserved variable (passengers). The transition is reminiscent of the condensation transition described earlier [11], and has also been useful in describing *clogging* in the transport of sticky particles down a pipe [20].

2.2.3. *Granular packing*

As a final example, we consider the packing of granular materials, which is important in many technological processes. The crucial issue in these problems is understanding the complex network of forces which is responsible for the static structure and properties of granular materials. One such system which has been subjected to experiments, simulations, and analysis is a pack of spherical beads in a compression cell [6].

The bead pack is modeled as a regular lattice of sites, each having a particle of unit mass. The mechanisms which lead to the formation of force chains in the system are summarized in the rules defined below: (i) Each site i in layer D is connected to N sites j in layer $D+1$. (ii) Only vertical forces are considered explicitly. A fraction q_{ij} of the total weight supported by particle i in layer D is transmitted to particle j in layer $D+1$. Thus, the weight $W(D, i)$ supported by the particle at the ith site in layer D satisfies the stochastic equation

$$W(D+1, j) = 1 + \sum_i q_{ij}(D) W(D, i). \tag{11}$$

The $q_{ij}(D)$ are independently-distributed random variables which satisfy the constraint $\sum_j q_{ij} = 1$, required for enforcing the force-balance condition on each particle.

In general, the values of W at neighboring sites in layer D are not independent. The MF approximation of this model ignores these correlations. Defining a normalized weight variable $v = W/D$, we want to obtain the force distribution $P_D(v)$, i.e., the probability that a site at depth D is subject to a vertical force v. Within the MF approximation, it is possible

to obtain a recursive equation for $P_D(v)$. Coppersmith et al. [6] found that, for almost all distributions of q, the distribution of forces decays exponentially. However, a power-law decay was also observed in some cases.

3. Fragmentation and aggregation of k-chips

3.1. *1-chip model*

Let us first consider the 1-chip model. The chipping kernel has the simple form

$$g_m(n) = w\delta_{n,1}. \tag{12}$$

With the above kernel, Equations (1) and (2) become

$$\frac{\mathrm{d}}{\mathrm{d}t}P(m,t) = -P(m,t)\sum_{m_1=1}^{m} w\delta_{m_1,1} - P(m,t)\sum_{m_2=1}^{\infty} P(m_2,t)\sum_{m_1=1}^{m_2} w\delta_{m_1,1} + \sum_{m_1=1}^{\infty} P(m+m_1,t)w\delta_{m_1,1} + \sum_{m_1=1}^{m} P(m-m_1,t)\sum_{m_2=m_1}^{\infty} P(m_2,t)w\delta_{m_1,1}, \quad m \geq 1, \tag{13}$$

$$\frac{\mathrm{d}}{\mathrm{d}t}P(0,t) = -P(0,t)\sum_{m_2=1}^{\infty} P(m_2,t)\sum_{m_1=1}^{m_2} w\delta_{m_1,1} + \sum_{m_1=1}^{\infty} P(m_1,t)w\delta_{m_1,1}. \tag{14}$$

Absorbing w into the definition of time, these equations simplify to the following form:

$$\frac{\mathrm{d}}{\mathrm{d}t}P(m,t) = -(1+s_1)P(m,t) + P(m+1,t) + s_1P(m-1,t), \quad m \geq 1, \tag{15}$$

$$\frac{\mathrm{d}}{\mathrm{d}t}P(0,t) = -s_1P(0,t) + P(1,t). \tag{16}$$

Here, we have defined $s_1(t) = \sum_{m=1}^{\infty} P(m,t)$ as the probability of occupancy of a site with mass $m \geq 1$. Consequently, the probability of a site being empty is $P(0,t) = 1 - s_1(t)$.

The above rate equations were obtained earlier in [11,12] and were solved exactly. We recall this calculation to illustrate the *generating-function approach* for obtaining steady-state solutions of such rate equations. Defining the generating function $Q(z,t) = \sum_{m=1}^{\infty} z^m P(m,t)$, an equation for $\partial Q/\partial t$ can be obtained from Equation (15) by multiplying both sides by z^m and summing over m:

$$\begin{aligned}\frac{\partial}{\partial t}Q(z,t) &= \frac{\partial}{\partial t}\sum_{m=1}^{\infty} z^m P(m,t)\\ &= -(1+s_1)\sum_{m=1}^{\infty} z^m P(m,t) + \sum_{m=1}^{\infty} z^m P(m+1,t) + s_1\sum_{m=1}^{\infty} z^m P(m-1,t)\\ &= -(1+s_1)Q + \frac{1}{z}\sum_{m=2}^{\infty} z^m P(m,t) + s_1 z\sum_{m=0}^{\infty} z^m P(m,t)\\ &= -(1+s_1)Q + \frac{1}{z}[Q - zP(1,t)] + s_1 z[Q + P(0,t)].\end{aligned} \tag{17}$$

Setting $\partial Q/\partial t = 0$, and substituting $P(1) = s_1(1 - s_1)$ from the steady-state version of Equation (16), we obtain

$$Q(z) = \frac{s_1(1 - s_1)z}{(1 - s_1 z)}. \tag{18}$$

The value of s_1 is fixed by mass conservation, which requires that $\sum_{m=1}^{\infty} mP(m) = \rho$, where ρ is the mass density. Putting $\mathrm{d}Q/\mathrm{d}z|_{z=1} = \rho$, we obtain

$$\rho = \frac{s_1}{1 - s_1} \quad \text{or} \quad s_1 = \frac{\rho}{1 + \rho}. \tag{19}$$

The steady-state distribution $P(m)$ is the coefficient of z^m in $Q(z)$, and can be obtained by Taylor-expanding $Q(z)$ about $z = 0$. This yields

$$P(m) = (1 - s_1)s_1^m, \quad m \geq 1. \tag{20}$$

For a more complicated function $Q(z)$, we can obtain $P(m)$ by inverting $Q(z)$. It is useful to illustrate this for the simple form of $Q(z)$ in Equation (18). Thus,

$$P(m) = \frac{1}{2\pi i}\int_C \mathrm{d}z \frac{Q(z)}{z^{m+1}}, \quad m \geq 1. \tag{21}$$

Here, the closed contour C encircles the origin in the complex plane counter-clockwise and lies inside the circle $|z| = 1/s_1$. The integral is calculated using the residue theorem. Only those singular points which lie within C (namely, $z = 0$, which is a pole of order m) contribute to this evaluation. The associated residue is

$$\mathrm{Res}\, f_1(z = 0) = \frac{1}{(m-1)!}\frac{\mathrm{d}^{m-1}}{\mathrm{d}z^{m-1}}\left(\frac{Q(z)}{z}\right)\bigg|_{z=0} \tag{22}$$

$$= (1 - s_1)s_1^m. \tag{23}$$

Thus, the steady-state mass distribution is

$$P(m) = \frac{1}{2\pi i} \cdot 2\pi i\, \mathrm{Res} f_1(0) = (1 - s_1)s_1^m, \quad m \geq 1. \tag{24}$$

Notice that $P(0) = 1 - s_1$, so Equation (24) is also valid for $P(0)$.

Using Equation (19), the above mass distribution can be rewritten as

$$P(m) = \frac{1}{1 + \rho}\left(\frac{\rho}{1 + \rho}\right)^m \equiv ae^{-bm}, \tag{25}$$

where

$$a = \frac{1}{1 + \rho}, \quad b = \ln\left(\frac{1 + \rho}{\rho}\right). \tag{26}$$

In the case of simple chipping kernels, as in Equation (12), the above solution can also be obtained directly from the difference equations (15) and (16) by setting the left-hand-side (LHS) to zero. We can then write down expressions for the first few

terms of $P(m)$:

$$\begin{aligned}
P(1) &= s_1 P(0) = s_1 - s_1^2, \\
P(2) &= (1+s_1)P(1) - s_1 P(0) \\
&= s_1^2 P(0) = s_1^2 - s_1^3, \\
P(3) &= (1+s_1)P(2) - s_1 P(1) \\
&= s_1^3 P(0) = s_1^3 - s_1^4, \\
&\cdot \\
P(m) &= (1+s_1)P(m-1) - s_1 P(m-2) \\
&= s_1^m P(0) = s_1^m - s_1^{m+1},
\end{aligned} \tag{27}$$

which is identical to Equation (24). Again, the mass conservation condition $\sum_{m=1}^{\infty} mP(m) = \rho$ results in Equation (19), as expected.

The 1-chip solution in Equation (25) is important because of its universal nature. As a matter of fact, it is a steady-state solution for all MF models where the chipping kernel $g_m(n)$ is independent of the mass of the departure site m, $g_m(n) = g(n)$. To confirm this, we consider Equations (1) and (2) with $g_m(n)$ replaced by $g(n)$. The corresponding rate equations are

$$\begin{aligned}
\frac{\mathrm{d}}{\mathrm{d}t}P(m,t) = &-P(m,t)\sum_{m_1=1}^{m} g(m_1) - P(m,t)\sum_{m_2=1}^{\infty} P(m_2,t)\sum_{m_1=1}^{m_2} g(m_1) \\
&+ \sum_{m_1=1}^{\infty} P(m+m_1,t)\,g(m_1) \\
&+ \sum_{m_1=1}^{m} P(m-m_1,t)\sum_{m_2=m_1}^{\infty} P(m_2,t)\,g(m_1), \quad m \geq 1,
\end{aligned} \tag{28}$$

$$\frac{\mathrm{d}}{\mathrm{d}t}P(0,t) = -P(0,t)\sum_{m_2=1}^{\infty} P(m_2,t)\sum_{m_1=1}^{m_2} g(m_1) + \sum_{m_1=1}^{\infty} P(m_1,t)\,g(m_1). \tag{29}$$

In the steady state, the above equations may be combined to obtain

$$\begin{aligned}
&-P(m)\sum_{m_1=1}^{m} g(m_1) - P(m)\frac{1}{P(0)}\sum_{m_1=1}^{\infty} P(m_1)\,g(m_1) \\
&+ \sum_{m_1=1}^{\infty} P(m+m_1)\,g(m_1) + \sum_{m_1=1}^{\infty} P(m-m_1)\sum_{m_2=m_1}^{\infty} P(m_2)\,g(m_1) = 0.
\end{aligned} \tag{30}$$

Substituting $P(m) = a\exp(-bm)$ on the RHS of Equation (30), we obtain

$$\begin{aligned}
\mathrm{RHS} = &\sum_{m_1=1}^{m} g(m_1) - \frac{1}{a}\sum_{m_1=1}^{\infty} ae^{-bm_1}g(m_1) + \sum_{m_1=1}^{\infty} e^{-bm_1}g(m_1) \\
&+ \sum_{m_1=1}^{\infty}\sum_{m_2=m_1}^{\infty} ae^{-b(m_2-m_1)}g(m_1).
\end{aligned} \tag{31}$$

The first and fourth terms cancel, and the second and third terms cancel, so $\mathrm{RHS} = 0$. This confirms that $P(m) = ae^{-bm}$ is a solution of Equations (28) and (29). The constants a and b are fixed by the requirements of probability normalization ($\sum_{m=0}^{\infty} P(m) = 1$) and

mass conservation ($\sum_{m=1}^{\infty} mP(m) = \rho$). We leave it as an exercise to the reader to verify that these conditions lead to the same values of a and b as in Equation (26).

Next, let us generalize the 1-chip model to a k-chip model, where $k > 1$. These k-chip models are interesting in physical situations where the deposited material consists of polymers or aggregates. We will see that the steady-state solutions for k-chip models exhibit a k-branch structure.

3.2. *2-chip model*

The steady-state distributions for the 2-chip model can be obtained using a procedure similar to the 1-chip model. The corresponding form of $g_m(n)$ is

$$g_m(n) = w\delta_{n,2}. \tag{32}$$

The rate equations in this case are (absorbing w into time t)

$$\frac{\mathrm{d}}{\mathrm{d}t}P(m,t) = -(1+s_2)P(m,t) + P(m+2,t) + s_2P(m-2,t), \quad m \geq 2, \tag{33}$$

$$\frac{\mathrm{d}}{\mathrm{d}t}P(m,t) = -s_2P(m,t) + P(m+2,t), \quad m < 2. \tag{34}$$

Here, $s_2(t) = \sum_{m=2}^{\infty} P(m,t)$ is the probability of sites having mass 2 or more. Notice that the kernel in Equation (32) is independent of the mass of the departure site. Thus, the 1-chip solution is a steady-state solution of Equations (33) and (34), as can be verified by direct substitution. However, an arbitrary initial condition $P(m,0)$ will not relax to this solution due to the presence of conserved quantities, as we shall see shortly.

The steady-state generating function $Q(z)$, obtained in analogy with the 1-chip case, is as follows:

$$Q(z) = \frac{z(s_1 - s_2) + z^2 s_2(1 - s_1)}{(1 - s_2 z^2)}, \tag{35}$$

where $s_2 = \sum_{m=2}^{\infty} P(m)$. It is straightforward to Taylor-expand $Q(z)$ in Equation (35) and identify $P(m)$. Alternatively, we can obtain $P(m)$ using Equation (21). Thus

$$P(m) = \frac{1}{2\pi i}\int_C \mathrm{d}z \frac{(s_1 - s_2) + s_2(1 - s_1)z}{z^m(1 - s_2 z^2)}, \quad m \geq 1. \tag{36}$$

In this case, the contour C encircles the origin counterclockwise, and lies inside the circle $|z| = 1/\sqrt{s_2}$. The singularities of the integrand $f_2(z)$ in the above equation are $z = 0$ (pole of order m), $z = 1/\sqrt{s_2}$ (simple pole) and $z = -1/\sqrt{s_2}$ (simple pole). The second and third poles lie outside C, making Res $f_2(z = 0)$ the only contributing residue. This evaluation yields

$$\text{Res } f_2(z=0) = \frac{(1 - s_1)}{2}[1 + (-1)^m]s_2^{m/2} + \frac{(s_1 - s_2)}{2}[1 - (-1)^m]s_2^{(m-1)/2}. \tag{37}$$

Thus, the steady-state probability distribution for the 2-chip model is given by

$$\begin{aligned} P(m) &= (1 - s_1)s_2^{m/2}\delta_{\mathrm{mod}(m,2),0} + (s_1 - s_2)s_2^{(m-1)/2}\delta_{\mathrm{mod}(m,2),1} \\ &\equiv P^{\mathrm{e}}(m) + P^{\mathrm{o}}(m). \end{aligned} \tag{38}$$

Here the function mod(m, n) is defined as the remainder on division of m by n. The first and second terms on the RHS of Equation (38) are the steady-state distributions for even values of m [$P^{e}(m)$] and odd values of m [$P^{o}(m)$], respectively. Thus, the 2-chip model has a steady-state solution comprising of two branches, both of which have the same exponential decay. Notice that the occupation probabilities for sites with even or odd units of mass are

$$S_{e} = \sum_{m=0,2,4,\ldots}^{\infty} P^{e}(m) = \frac{1 - s_1}{1 - s_2}, \tag{39}$$

$$S_{o} = \sum_{m=1,3,5,\ldots}^{\infty} P^{o}(m) = \frac{s_1 - s_2}{1 - s_2}. \tag{40}$$

These quantities remain conserved during the evolution because of the nature of the 2-chip move. The two branches appear as a consequence of these two conserved quantities.

The probabilities of occupancy s_1 and s_2 are related to the mass density ρ as follows:

$$\rho = \left.\frac{\mathrm{d}Q}{\mathrm{d}z}\right|_{z=1} = \frac{s_1 + s_2}{1 - s_2}. \tag{41}$$

As before, ρ may be calculated from either $Q(z)$ or $P(m)$. The quantities s_1 and s_2 can be determined in terms of ρ and S_{e} (or S_{o}):

$$s_1 = \frac{\rho - S_{e} + 1}{\rho + S_{e} + 1}, \quad s_2 = \frac{\rho + S_{e} - 1}{\rho + S_{e} + 1}. \tag{42}$$

It should be noted that $\rho + S_{e}$ is always greater than 1, ensuring that $s_2 > 0$. If we choose the initial conditions $P(m, 0)$ such that $s_2 = s_1^2$ in Equation (42), the branched solution of Equation (38) reduces to the 1-chip exponential solution. Alternatively, if we substitute $s_2 = s_1^2$ in Equation (35), we recover the generating function of the 1-chip model in Equation (18).

3.3. *k-chip model*

In general, consider the case of k units of mass chipping from a site and then aggregating with the mass of a randomly-chosen nearest neighbor we get

$$g_m(n) = w\delta_{n,k}. \tag{43}$$

The corresponding rate equations for $P(m, t)$, obtained by substituting Equation (43) in Equations (1) and (2), are as follows (absorbing w into t):

$$\frac{\mathrm{d}}{\mathrm{d}t}P(m, t) = -(1 + s_k)P(m, t) + P(m + k, t) + s_k P(m - k, t), \quad m \geq k, \tag{44}$$

$$\frac{\mathrm{d}}{\mathrm{d}t}P(m, t) = -s_k P(m, t) + P(m + k, t), \quad m < k. \tag{45}$$

Here, $s_k(t) = \sum_{m=k}^{\infty} P(m, t)$ is the probability of sites having mass k or more. As the kernel in Equation (43) is independent of the mass of the departure site, $P(m) = a\exp(-bm)$ is a steady-state solution of Equations (44) and (45). However, as in the 2-chip case, an arbitrary initial condition $P(m, 0)$ will not relax to this exponential solution due to the

presence of k conserved quantities: $\sum_{m=0}^{\infty} P(n+mk, t)$ with $n = 0, 1, \ldots, k-1$. Rather, the steady-state solution will consist of k branches.

The steady-state generating function for the k-chip model is

$$Q(z) = \frac{z(s_1 - s_2) + z^2(s_2 - s_3) + \cdots + z^k s_k(1 - s_1)}{(1 - s_k z^k)}, \tag{46}$$

where $s_k = \sum_{m=k}^{\infty} P(m)$. The corresponding probability distribution is as follows:

$$P(m) = (1 - s_1)s_k^{m/k}\delta_{\mathrm{mod}(m,k),0} + (s_1 - s_2)s_k^{(m-1)/k}\delta_{\mathrm{mod}(m,k),1} + \cdots + (s_i - s_{i+1})s_k^{(m-i)/k}\delta_{\mathrm{mod}(m,k),i} + \cdots + (s_{k-1} - s_k)s_k^{(m-k+1)/k}\delta_{\mathrm{mod}(m,k),k-1}. \tag{47}$$

For completeness, we present the derivation of Equation (47) for the 3-chip case in Appendix B. The s_i's are related to the mass density via the relation

$$\rho = \frac{s_1 + s_2 + \cdots + s_k}{1 - s_k}. \tag{48}$$

Thus, the steady-state solution for the k-chip model consists of k branches. All the branches in the probability distribution of Equation (47) decay exponentially with a slope $\ln(s_k)/k$. The quantities $s_1, \ldots, s_k$ are determined from Equation (48) plus the $(k-1)$ conserved probability sums in the branches

$$S_i = \sum_{m=i,i+k,\ldots}^{\infty} (s_i - s_{i+1})s_k^{(m-i)/k} = \frac{s_i - s_{i+1}}{1 - s_k}, \quad i = 0, 1, \ldots, k-1. \tag{49}$$

Notice that one of the S_i's (say, S_{k-1}) is not independent because $\sum_{i=0}^{k-1} S_i = 1$. Further, appropriately chosen initial conditions resulting in steady-state values $s_2 = s_1^2$, $s_3 = s_1^3, \ldots, s_k = s_1^k$ collapse the k branches in Equation (47) to the 1-chip solution.

Before concluding this section, let us make an observation about the k-chip lattice model, i.e., the original model rather than its "rate equation" counterpart. This model has an exponentially large set of disjoint sectors, and configurations in different sectors are not connected by the dynamics. To see this, we denote the number of particles on a site i as m_i. As k particles arrive at or leave this site at a given time, the quantity $M_i = \mathrm{mod}(m_i, k)$ is conserved. Therefore, the set $\{M_i\}$ is conserved by the dynamics, and labels a particular sector. The number of sectors is k^N, where N is the number of lattice sites. Such systems have been referred to as *many-sector decomposable systems* by Menon et al. [23].

4. MC simulations

In this section, we present MC results for some of the models discussed earlier. All simulations were performed on 1-d and 2-d lattices with periodic boundary conditions. The lattice sizes were $L = 1024$ (in $d = 1$) and $L^2 = 128 \times 128$ (in $d = 2$). The data presented here was obtained as an average over 500 independent runs. The details of the MC procedure are provided in Appendix C, so that the reader can implement these models numerically.

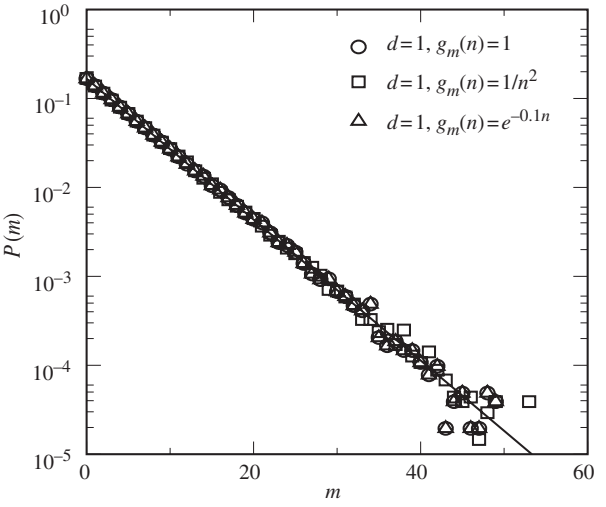

Figure 2. Steady-state probability distributions ($P(m)$ *vs.* m) from 1-d MC simulations with three different functional forms for the chipping kernel $g_m(n)$. The data sets are plotted on a linear-logarithmic scale. The details of the MC simulations are provided in the text. The mass density for the initial conditions is $\rho = 5$. The solid line denotes the 1-chip solution in Equation (25).

First, we present results for chipping kernels which satisfy $g_m(n) = g(n)$, discussed at the end of Section 3.1. In Figure 2, we plot $P(m)$ *versus* m obtained from 1-d MC simulations with three different functional forms of $g_m(n)$:

$$\begin{aligned} g_m(n) &= 1, \\ g_m(n) &= \frac{1}{n^2}, \\ g_m(n) &= e^{-0.1n}. \end{aligned} \tag{50}$$

The MC data sets are numerically coincident with each other as well as the 1-chip solution in Equation (25) (denoted as a solid line), which was obtained from the corresponding MF equations. The mass density in each case was $\rho = 5$. There is an excellent agreement between the different data sets, showing that the MC data is described very well by the solutions of the corresponding MF equations, even for $d = 1$. This feature is also observed in our subsequent results, suggesting that the MF equations are exact in the present context [22].

Next, we present results for the 2-chip model discussed in Section 3.2. Figure 3(a) shows the steady-state distribution obtained from 1-d and 2-d MC simulations for initial conditions with $\rho = 10$, and $S_e = 1$, $S_o = 0$. The solid line denotes the result in Equation (38) with values of s_1 and s_2 evaluated from Equation (42). As our initial condition only had sites with even m populated, the steady-state solution is the even-m branch of Equation (38). Figure 3(b) is similar, but for a mixed initial condition with $\rho = 9.5$ and $S_e = S_o = 1/2$. The branched nature of the solution, resulting in a staircase-type probability distribution, is highlighted in the inset.

In Figure 4, we show the steady-state distributions obtained from 1-d and 2-d MC simulations of the 3-chip model. In Figure 4(a), the initial condition had $P(9,0) = P(10,0) = P(11,0) = 1/3$. This corresponds to $\rho = 10$, and all three branches are equally populated. The solid line in Figure 4(a) denotes the result in Equation (47) with s_1, s_2, and

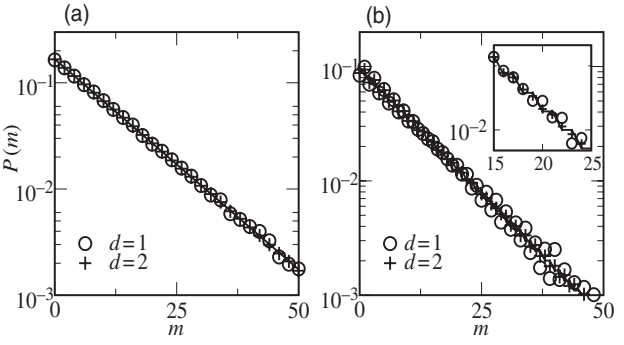

Figure 3. Steady-state distributions for the 2-chip model, obtained from MC simulations. (a) Plot of $P(m)$ vs. m on a linear-log scale, from MC simulations in $d=1,2$. The initial conditions were characterized by average density $\rho=10$, and $S_e=1$, $S_o=0$. The solid line denotes the solution in Equation (38) with $s_1=s_2=\rho/(\rho+2)$. (b) Analogous to (a), but the initial conditions for the MC simulations have a mixture of both even and odd masses. The corresponding parameter values are $\rho=9.5$, $S_e=S_o=1/2$. The solid line denotes the solution in Equation (38) with $s_1=(2\rho+1)/(2\rho+3)$, $s_2=(2\rho-1)/(2\rho+3)$. The inset highlights the staircase structure of the probability distribution.

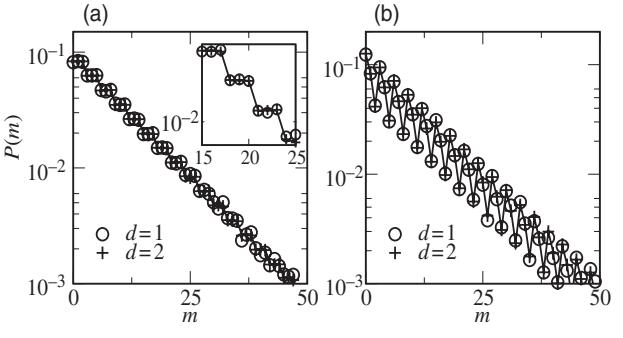

Figure 4. Analogous to Figure 3, but for the 3-chip model. (a) Plot of $P(m)$ *vs.* m from MC simulations with $P(9,0)=P(10,0)=P(11,0)=1/3$, so that $\rho=10$. The solid line denotes the result in Equation (47) with s_1, s_2, and s_3 calculated from Equation (B6) as $s_1=0.917$, $s_2=0.833$, $s_3=0.75$. (b) Plot of $P(m)$ *vs.* m for initial conditions with $P(9,0)=1/2$, $P(10,0)=1/3$, $P(11,0)=1/6$, so that $\rho\simeq 9.67$. The solid line denotes the result in Equation (47) with $s_1=0.875$, $s_2=0.792$, $s_3=0.75$.

s_3 calculated from Equation (B6). Figure 4(b) is analogous to Figure 4(a), but the initial condition now has $P(9,\,0)=1/2$, $P(10,\,0)=1/3$, and $P(11,\,0)=1/6$. The corresponding value of the average density is $\rho\simeq 9.67$. Again, in both sets of figures, the MC simulations agree very well with the corresponding MF result.

5. Summary and discussion

Let us conclude this article with a summary and discussion. There has been much research interest in mass-transport models, which arise in many physical contexts. Therefore, we believe it is appropriate to make this subject accessible to a wider audience. This is the underlying motivation for this article. For the purposes of this exposition, we focus

on fragmentation–aggregation models with conserved mass, i.e., there is no ongoing adsorption or desorption. We consider models with the chipping rate $g_m(n)$, where n is the chipped mass and m is the mass of the departure site. We use the corresponding MF equations to obtain the steady-state probability distributions ($P(m)$ *vs.* m) for different functional forms of $g_m(n)$. We show that a large class of chipping kernels, where $g_m(n)$ is independent of m, give rise to an exponentially-decaying distribution: $P(m) = a \exp(-bm)$. This is also the MF solution for the 1-chip model (cf. Equation (25)), where one unit of mass fragments from a site and aggregates with a randomly-chosen nearest-neighbor.

We have also discussed k-chip models for fragmentation and aggregation. The resulting steady-state distribution has k branches, each of which decays exponentially with the same slope. This slope is determined by the average density ρ, and the population of the branches in the initial condition $P(m, 0)$ for the rate equations (1) and (2). The initial population in each of the branches is conserved during the evolution, and is also reflected in the steady-state distribution.

Finally, we compared the MF analytical results with those from MC simulations in $d = 1, 2$. In all cases, we found that the MF results for $P(m)$ *versus* m were in excellent agreement with the MC results. This demonstrates that the MF results are exact in the present context.

There are many open research problems in the area of mass transport, aggregation, and growth. These models can be tackled with a wide range of analytical and numerical techniques, which are both simple and elegant. We hope that this review will motivate further studies of this fascinating area.

Acknowledgements

The authors would like to thank M. Barma, S.N. Majumdar and R. Rajesh for fruitful discussions. G.P. Shrivastav and V. Banerjee would like to acknowledge the support of CSIR Grant No. 03(1077)/06/EMR-II. S. Puri is grateful to the Department of Science and Technology, India, for supporting this work through the project *Pattern Formation in Granular Materials*.

References

[1] M. Lagally, *Kinetics of Ordering and Growth at Surfaces*, Vol. 239 of NATO Advanced Study Institute, Series B: Physics, Plenum, New York, 1990.
[2] Z. Zang and M. Lagally, *Morphological Organization of Epitaxial Growth and Removal*, World Scientific, Singapore, 1998.
[3] W.H. White, *On the form of steady-state solutions to the coagulating equations*, J. Colloid Interface Sci. 87 (1982), pp. 204–208.
[4] R.M. Ziff, *Kinetics of polymerization*, J. Stat Phys. 23 (1980), pp. 241–263.
[5] A.E. Scheidegger, Int. Assoc. Sci. Hydrol. Bull. 12 (1967), p. 15.
[6] S.N. Coppersmith, C.-h. Liu, S. Majumdar, O. Narayan, and T.A. Witten, *Model for force fluctuations in bead packs*, Phys. Rev. E 53 (1996), pp. 4673–4685.
[7] J. Krug and J. Garcia, *Asymmetric particle systems on* $\mathbb{R}$, J. Stat. Phys. 99 (2000), pp. 31–55.
[8] J. Marro and R. Dickman, *Nonequilibrium Phase Transitions in Lattice Models*, Cambridge University Press, Cambridge, 1999.
[9] H. Hinrichsen, *Non-equilibrium critical phenomena and phase transitions into absorbing states*, Adv. Phys. 49 (2000), pp. 815–918.

[10] P.L. Krapivsky, J.F.F. Mendes, and S. Redner, *Influence of island diffusion on submonolayer epitaxial growth*, Phys. Rev. B 59 (1999), pp. 15950–15958.
[11] S.N. Majumdar, S. Krishnamurthy, and M. Barma, *Nonequilibrium phase transition in a model of diffusion, aggregation and fragmentation*, J. Stat. Phys. 99 (2000), pp. 1–29.
[12] R. Rajesh, D. Das, B. Chakraborty, and M. Barma, *Aggregate formation in a system of coagulating and fragmenting particles with mass-dependent diffusion rates*, Phys. Rev. E 66 (2002), p. 056104.
[13] E. Levine, D. Mukamel, and G. Ziv, *The condensation transition in zero-range processes with diffusion*, J. Stat. Mech.: Theory Exp. (2004), p. P05001.
[14] (a) K. Binder, *Monte Carlo Methods in Statistical Physics*, Springer-Verlag, Berlin, 1986; (b) K. Binder and D.W. Heermann, *Monte Carlo Simulations in Statistical Physics: An Introduction*, Springer-Verlag, Berlin, 1988.
[15] M.E.J. Newman and G.T. Barkema, *Monte Carlo Methods in Statistical Physics*, Oxford University Press, Oxford, 1999.
[16] S. Odenbach, *Ferrofluids – Magnetically controlled fluids and their applications*, Springer-Verlag, Berlin, 2002.
[17] Q.A. Pankhurst, J. Connolly, S.K. Jones, and J. Dobson, *Applications of magnetic nanoparticles in biomedicine*, J. Phys. D: Appl. Phys. 36 (2003), pp. R167–R181.
[18] R.E. Rosensweig, *Ferrohydrodynamics*, Dover Publications, New York, 1997.
[19] P.L. Krapivsky and S. Redner, *Transitional aggregation kinetics in dry and damp environments*, Phys. Rev. E 54 (1996), pp. 3553–3561.
[20] O.J. O'Loan, M.R. Evans, and M.E. Cates, *Jamming transition in a homogeneous one-dimensional system: The bus route model*, Phys. Rev. E 58 (1998), pp. 1404–1418.
[21] M.R. Evans, *Phase transitions in one-dimensional nonequilibrium systems*, Braz. J. Phys. 30 (2000), pp. 42–57.
[22] M.R. Evans, S.N. Majumdar, and R.K.P. Zia, *Factorized steady states in mass transport models*, J. Phys. A 37 (2004), pp. L275–L280.
[23] G.I. Menon, M. Barma, and D. Dhar, *Conservation laws and integrability of one-dimensional model of diffusing dimers*, J. Stat. Phys. 86 (1997), pp. 1237–1263.

Appendix A: Verification of the sum rule on $P(m,t)$

We want to show that $\mathrm{d}\left[\sum_{m=0}^{\infty} P(m,t)\right]/\mathrm{d}t = 0$. Using Equations (1) and (2),

$$\begin{aligned}
\frac{\mathrm{d}}{\mathrm{d}t}\left[\sum_{m=0}^{\infty} P(m,t)\right] &= \frac{\mathrm{d}}{\mathrm{d}t}\left[\sum_{m=1}^{\infty} P(m,t) + P(0,t)\right] \\
&= -\sum_{m=1}^{\infty} P(m,t) \sum_{m_1=1}^{m} g_m(m_1) - \sum_{m=1}^{\infty} P(m,t) \sum_{m_2=1}^{\infty} P(m_2,t) \sum_{m_1=1}^{m_2} g_{m_2}(m_1) \\
&\quad + \sum_{m=1}^{\infty} \sum_{m_1=1}^{\infty} P(m+m_1,t)\, g_{m+m_1}(m_1) \\
&\quad + \sum_{m=1}^{\infty} \sum_{m_1=1}^{m} P(m-m_1,t) \sum_{m_2=m_1}^{\infty} P(m_2,t)\, g_{m_2}(m_1) \\
&\quad - P(0,t) \sum_{m_2=1}^{\infty} P(m_2,t) \sum_{m_1=1}^{m_2} g_{m_2}(m_1) + \sum_{m_1=1}^{\infty} P(m_1,t)\, g_{m_1}(m_1). \qquad \text{(A1)}
\end{aligned}$$

We regroup terms and write

$$\begin{aligned}
\text{LHS} = &-\sum_{m=1}^{\infty} P(m,t) \sum_{m_1=1}^{m} g_m(m_1) \\
&+ \Bigg[-\sum_{m=1}^{\infty} P(m,t) \sum_{m_2=1}^{\infty} P(m_2,t) \sum_{m_1=1}^{m_2} g_{m_2}(m_1) \\
&- P(0,t) \sum_{m_2=1}^{\infty} P(m_2,t) \sum_{m_1=1}^{m_2} g_{m_2}(m_1) \Bigg] \\
&+ \Bigg[\sum_{m=1}^{\infty} \sum_{m_1=1}^{\infty} P(m+m_1,t)\, g_{m+m_1}(m_1) + \sum_{m_1=1}^{\infty} P(m_1,t)\, g_{m_1}(m_1) \Bigg] \\
&+ \sum_{m=1}^{\infty} \sum_{m_1=1}^{m} P(m-m_1,t) \sum_{m_2=m_1}^{\infty} P(m_2,t)\, g_{m_2}(m_1) \qquad \text{(A2)} \\
= &-\sum_{m=1}^{\infty} P(m,t) \sum_{m_1=1}^{m} g_m(m_1) - \sum_{m=0}^{\infty} P(m,t) \sum_{m_2=1}^{\infty} P(m_2,t) \sum_{m_1=1}^{m_2} g_{m_2}(m_1) \\
&+ \sum_{m=0}^{\infty} \sum_{m_1=1}^{\infty} P(m+m_1,t)\, g_{m+m_1}(m_1) \\
&+ \sum_{m=1}^{\infty} \sum_{m_1=1}^{m} P(m-m_1,t) \sum_{m_2=m_1}^{\infty} P(m_2,t)\, g_{m_2}(m_1). \qquad \text{(A3)}
\end{aligned}$$

Our initial condition for Equations (1) and (2) satisfies $\sum_{m=0}^{\infty} P(m,0) = 1$. Therefore, we set $\sum_{m=0}^{\infty} P(m,t) = 1$ on the RHS of Equation (A3). This is justified subsequently as it results in $\mathrm{d}\left[\sum_{m=0}^{\infty} P(m,t)\right]/\mathrm{d}t = 0$. Thus

$$\begin{aligned}
\text{LHS} = &-\sum_{m=1}^{\infty} P(m,t) \sum_{m_1=1}^{m} g_m(m_1) - \sum_{m_2=1}^{\infty} P(m_2,t) \sum_{m_1=1}^{m_2} g_{m_2}(m_1) \\
&+ \sum_{m_1=1}^{\infty} \sum_{m_2=m_1}^{\infty} P(m_2,t)\, g_{m_2}(m_1) \\
&+ \sum_{m_1=1}^{\infty} \sum_{m=m_1}^{\infty} P(m-m_1,t) \sum_{m_2=m_1}^{\infty} P(m_2,t)\, g_{m_2}(m_1) \qquad \text{(A4)} \\
= &-2 \sum_{m=1}^{\infty} P(m,t) \sum_{m_1=1}^{m} g_m(m_1) + 2 \sum_{m_1=1}^{\infty} \sum_{m_2=m_1}^{\infty} P(m_2,t)\, g_{m_2}(m_1). \qquad \text{(A5)}
\end{aligned}$$

In the second term on the RHS of Equation (A5), we interchange the order of the summations over m_1 and m_2. This leads to a cancellation of the two terms, proving that $\mathrm{d}\left[\sum_{m=0}^{\infty} P(m,t)\right]/\mathrm{d}t = 0$.

Appendix B: Steady-state distribution for the 3-chip model

The generating function for the 3-chip model is (cf. Equation (46))

$$Q(z) = \frac{(s_1 - s_2)z + (s_2 - s_3)z^2 + s_3(1 - s_1)z^3}{(1 - s_3 z^3)}, \qquad \text{(B1)}$$

where $s_3 = \sum_{m=3}^{\infty} P(m)$. From Equation (21), we have

$$P(m) = \frac{1}{2\pi i} \int_C \mathrm{d}z \frac{(s_1 - s_2)z + (s_2 - s_3)z^2 + s_3(1 - s_1)z^3}{z^{m+1}(1 - s_3 z^3)}, \quad m \geq 1. \qquad \text{(B2)}$$

The closed contour C encircles the origin and lies inside the region defined by $|z| < 1/{s_3}^{1/3}$. As usual, only Res $f_3(z=0)$ contributes to the integral, and is evaluated as

$$\begin{aligned}
\text{Res } f_3(z=0) &= \frac{1}{(m-1)!}\frac{\mathrm{d}^{m-1}}{\mathrm{d}z^{m-1}}\left(\frac{Q(z)}{z}\right)\Bigg|_{z=0} \\
&= \frac{1}{(m-1)!}\frac{\mathrm{d}^{m-1}}{\mathrm{d}z^{m-1}}\left[\frac{(s_1-s_2)+(s_2-s_3)z+s_3(1-s_1)z^2}{(-s_3)(z^3-1/s_3)}\right]\Bigg|_{z=0} \\
&= \frac{(1-s_1)}{3}\left[1+2\cos\left(\frac{2\pi(m-3)}{3}\right)\right]s_3^{m/3} \\
&\quad + \frac{(s_1-s_2)}{3}\left[1+2\cos\left(\frac{2\pi(m-1)}{3}\right)\right]s_3^{(m-1)/3} \\
&\quad + \frac{(s_2-s_3)}{3}\left[1+2\cos\left(\frac{2\pi(m-2)}{3}\right)\right]s_3^{(m-2)/3}. \qquad \text{(B3)}
\end{aligned}$$

Then, the steady-state mass distribution is

$$\begin{aligned}
P(m) &= \frac{(1-s_1)}{3}\left[1+2\cos\left(\frac{2\pi(m-3)}{3}\right)\right]s_3^{m/3} \\
&\quad + \frac{(s_1-s_2)}{3}\left[1+2\cos\left(\frac{2\pi(m-1)}{3}\right)\right]s_3^{(m-1)/3} \\
&\quad + \frac{(s_2-s_3)}{3}\left[1+2\cos\left(\frac{2\pi(m-2)}{3}\right)\right]s_3^{(m-2)/3} \\
&= (1-s_1){s_3}^{m/3}\delta_{\mathrm{mod}(m,3),0} + (s_1-s_2){s_3}^{(m-1)/3}\delta_{\mathrm{mod}(m,3),1} \\
&\quad + (s_2-s_3){s_3}^{(m-2)/3}\delta_{\mathrm{mod}(m,3),2}. \qquad \text{(B4)}
\end{aligned}$$

The relation between the mass density ρ and the s_i's can be obtained directly by using Equation (B4). Thus

$$\rho = \frac{s_1+s_2+s_3}{1-s_3}. \qquad \text{(B5)}$$

As for the 2-chip model, the s_i's can be obtained as a function of ρ and the probability sums on each of the branches in Equation (49). These result in the following expressions:

$$\begin{aligned}
s_1 &= \frac{\rho}{\rho+2+S_0-S_2} + \frac{2S_1+S_0S_2-S_1S_2}{(\rho+2+S_0-S_2)(1-S_2)}, \\
s_2 &= \frac{\rho}{\rho+2+S_0-S_2} + \frac{S_2-S_1}{\rho+2+S_0-S_2}, \\
s_3 &= \frac{\rho}{\rho+2+S_0-S_2} - \frac{S_1+S_2+S_0S_2-S_2^2}{(\rho+2+S_0-S_2)(1-S_2)}. \qquad \text{(B6)}
\end{aligned}$$

Appendix C: MC simulations of mass-transport models

1. *1-Chip model*

Consider a one-dimensional lattice with periodic boundary conditions and label the sites with integers $i=1,2,3,\ldots,L$. Fix the mass density ρ.

(1) Initializing the lattice: Integer masses m_i are placed on the lattice sites in accordance with the chosen ρ such that $\sum_{i=1}^{L} m_i = \rho L$. A simple procedure for achieving this is as follows:

   (a) Choose an integer random number NRAN(i) from the range $[0, L]$ for each site i.

(b) Assign $m_i = \text{Int}[(\rho+1)L * \text{NRAN}(i)/\sum_i \text{NRAN}(i)]$, where Int($x$) refers to the integer part of x.

(2) Chipping and aggregation: A site i is chosen at random. If m_i is non-zero, a unit mass chips and aggregates with a randomly-chosen neighbor. Thus $m_i \to m_i - 1$, and $m_{i-1} \to m_{i-1} + 1$ or $m_{i+1} \to m_{i+1} + 1$ with a probability 1/2.
(3) Repeat step 2 for L times, which corresponds to one MC step (MCS).
(4) Compute the mass distribution of lattice sites.
(5) Repeat steps 2–4 for several MCS, storing the mass distribution at intermediate MCS.
(6) Repeat steps 2–5 for a large number of independent lattice configurations, generated via step 1.
(7) Compute the configuration-averaged steady-state mass distribution, $P(m)$ *versus* m.

The steady state is achieved when the mass distribution does not change (apart from numerical fluctuations) in subsequent MCS.

2. *Case with $g_m(n) = 1/n^2$*

In general, the fragmentation rates $g_m(n)$ can be computed prior to the simulation and stored in a matrix for easy look-up using the following tips:

(1) Define a matrix G of dimension $N \times N$, chosen specific to $g_m(n)$. For example, if $g_m(n) = 1/n^2$, the rate of chipping a mass of size 1000 is 10^{-6}. We can assume that chipping of masses greater than 1000 occurs with a very small rate, and hence these events may be ignored. Thus we may set $N = 1000$.
(2) Initialize G_{mn} to zero. The row index m corresponds to the mass of the lattice site chosen to fragment. Masses greater than N may be treated as N for the computation of fragmentation rates for reasons discussed in 1 above. The column index refers to the chipped mass $n \le m$. Thus the matrix G has a triangular form, with the non-zero entries calculated using $g_m(n)$. For example, if $g_m(n) = 1/n^2$, the rates for the 10th row are $(1, 0.25, 0.1111, 0.0625, 0.04, 0.02777, 0.0204, 0.0156, 0.0123, 0.01, 0, 0, \ldots, 0)$. To connect these to probabilities, we normalize these numbers by $\sum_{n=1}^{\infty} 1/n^2$.

Once the look-up table for fragmentation rates is computed, the MC procedure is as before with step 2 replaced by the following steps.

(A) A site i is chosen at random. If m_i is non-zero, draw a random number r in the interval $(0, 1)$.
(B) Go to the m_ith row of the table and check the two consecutive entries which sandwich r. The column number of the larger entry is the number of mass particles n that chip from m_i. Thus $m_i \to m_i - n$, and $m_{i-1} \to m_{i-1} + n$ or $m_{i+1} \to m_{i+1} + n$ with probability 1/2.